RSC Advances

REVIEW

View Article Online
View Journal | View Issue

Cite this: *RSC Adv.*, 2023, **13**, 2140

Research progress of yolk–shell structured nanoparticles and their application in catalysis

Meiyu Si,[ab] Feng Lin,*[a] Huailan Ni,[a] Shanshan Wang,[b] Yaning Lu[ac] and Xiangyan Meng*[a]

Received 27th November 2022
Accepted 3rd January 2023

DOI: 10.1039/d2ra07541e

rsc.li/rsc-advances

Yolk–shell nanoparticles (YSNs) have attracted a broad interest in the field of catalysis due to their unique structure and properties. The hollow structure of YSNs brings high porosity and specific surface areas which is conducive to the catalytic reactions. The flexible tailorability and functionality of both the cores and shells allow a rational design of the catalyst and may have synergistic effect which will improve the catalytic performance. Herein, an overview of the research progress with respect to the synthesis and catalytic applications of YSNs is provided. The major strategies for the synthesis of YSNs are presented, including hard template method, soft template method, ship-in-a-bottle method, galvanic replacement method, Kirkendall diffusion method as well as the Ostwald ripening method. Moreover, we discuss in detail the recent progress of YSNs in catalytic applications including chemical catalysis, photocatalysis and electrocatalysis. Finally, the future research and development of YSNs are prospected.

1. Introduction

With the continuous research on materials science, nanomaterials with unique structure and function have attracted more and more attention, in which the yolk–shell structured nanoparticles (YSNs), or so-called rattle-typed structured nanoparticles become one of the most popular nanomaterials. The unique yolk–shell structure endows YSNs with excellent physical and chemical properties, showing great potential in many different fields, such as lithium-ion batteries, drug delivery, nanoreactor and catalysis. Indeed, the yolk–shell structure represents a special core–shell structure with movable core and functional shell, which can be more precisely described as core@void@shell structure. Compared with the conventional core–shell structure, the yolk–shell structure has lower density, larger space, higher specific surface area as well as stronger loading capacity.[1] The hard outer shell structure not only protects the inner core from agglomeration, but also allows the selective adsorption and enrichment of various reactants, promoting the reactions. The core of YSNs can move freely inside the cavity, which allows a full contact with the reactant and maximum exert its function. In addition, the cavity of YSNs will provide a confined space and can be also used as a storage or reaction chamber. According to the structure of core and shell, YSNs can be roughly divided into the following five different types:[2] (i) single core encapsulated in shell; (ii) multiple cores encapsulated in shell; (iii) core-satellite–shell structure; (iv) single yolk in shell with multiple cores loaded on shell surface; (v) single core within multiple shells (Fig. 1). Till now, many different synthetic strategies have been developed for the fabrication of YSNs. Among those, the hard template method is considered to be the simplest and effective approach, in which a layer of template material will be first coated on a hard-core surface, followed by coating with the target shell material, and YSNs will be obtained after sacrificing the template layer. The soft template method is quite similar with that of the hard template method, except for using vesicles formed by the self-assembly of amphoteric molecules (including surfactants and block copolymers) as the sacrificial

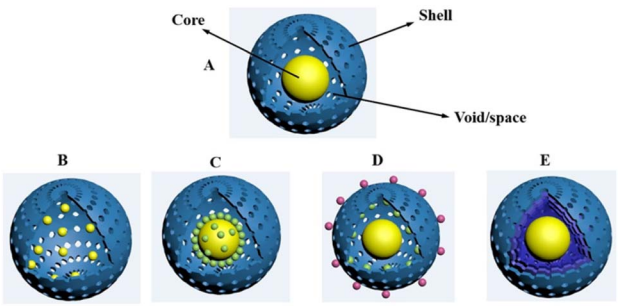

Fig. 1 Diagram of different types of YSNs. (A) Single core encapsulated in shell; (B) multiple cores encapsulated in shell; (C) core-satellite–shell structure; (D) single yolk in shell with multiple cores loaded on shell surface; (E) single core within multiple shells.

[a]Department of Chemistry and Chemical Engineering, Heze University, Heze 274015, Shandong Province, China. E-mail: linfeng@hezeu.edu.cn; mengxiangyan@hezeu.edu.cn

[b]School of Marine Science and Technology, Harbin Institute of Technology at Weihai, Weihai 264209, Shandong Province, China

[c]School of Chemistry and Chemical Engineering, University of Jinan, Jinan 250022, Shandong Province, China

template, which can easily be removed afterwards. Besides, a series of self-template approaches have been developed without the use of additional structural guiding template, such as the galvanic replacement method, Kirkendall diffusion method and Ostwald ripening method.[3]

The development of high efficiency, low cost and environmentally friendly catalyst has been considered to be the main desire in the field of catalysis. Due to its unique structure and properties, YSNs have practical significance in nanocatalysis, magnetic assisted catalysis, integrated catalysis and so on.[3] On the one hand, the hollow structure of YSNs brings it with high porosity and specific surface areas which is conducive to the catalysis reactions. On the other hand, the different composition of the core and shell may have synergistic effect which will improve its catalytic activity and selectivity. Moreover, the combination of the properties of core and shell can greatly extend the application fields, for example, magnetic materials@catalytic materials can be used for many times while maintaining their activity,[4] improving their recycling efficiency and adapting to green and sustainable development.

Herein, we introduce in detail the synthesis and catalytic application of YSNs. Firstly, we give a comprehensive overview of the synthesis strategies: hard template method, soft template method, ship-in-a-bottle method, galvanic replacement method, Kirkendall diffusion method as well as Ostwald ripening method. All strategies are very effective and have their own set of advantages that will lead to YSNs with the certain composition and structure. Then, we focus on the state of the art of YSNs in catalysis applications, including chemical catalysis, photocatalysis and electrocatalysis. At last, the future research and development of YSNs are prospected.

2. Synthetic strategies for YSNs

2.1 Hard template

Hard template method is one of the most universal methods for preparing almost all types of YSNs materials.[5,6] As shown in Fig. 2, in this approach, the pre-synthesized core is first coated with one or two layers of hard template to form a core–shell or sandwich-like structure, respectively. Then, the template (core, shell, or middle layer) can be selectively removed by calcination, chemical etching or solvent dissolution to create a cavity between the core and outer-layer shell.

2.1.1 Partial removal of the core. In this method, YSNs are obtained by partially removing of the core from above mentioned core–shell structure. For example, Lee at al. fabricated Au@SiO_2 YSNs through partial etching of the Au core inside SiO_2 shell.[7] Au particles are first coated with SiO_2 shell by using the traditional stÖber method and followed by KCN treatment, the reaction is as follows: $4Au + 8CN^- + O_2 + H^+ \rightarrow 4Au(CN)_2^- + 2H_2O$. Therefore, a yolk–shell structure can be formed as the size of the gold core becomes smaller (Fig. 3). By using a similar method, Kim and co-workers fabricated MF@SiO_2 YSNs in which the Melamine formaldehyde (MF) core is partially dissolved through an alkali treatment with ammonium hydroxide (NH_4OH). Furthermore, they used MF@SiO_2 YSNs to encapsulate gold nanoparticles selectively and loaded the gold particles on the MF cores.[8]

2.1.2 Partial removal of the shell. Partial shell dissolution method is one of the most common methodologies for the production of YSNs. Luo *et al.* developed a new oxidative linker cleaving (OLC) process, which used 2,5-dinhyopoxyterephthalicacid (DOBDC) as a sacrificial linker and selectively cleaved it into small molecular fragments by oxidative ring-opening reaction.[9] During the synthesis of UiO-66-$(OH)_2$, polyvinylpyrrolidone (PVP) coated Pd NPs with an average size of 25 nm were introduced, after 1.5 h in peroxymonosulfate (PMS) solution, reactive oxygen species (ROS) were generated around the pre-embedded Pd NPs, which could be generated by catalytic activation of PMS under acidic, neutral or alkaline conditions by various metal ions, metal NPs, alloy NPs and metal oxides, resulting in isolated cavities around each Pd NPs. Therefore, the OLC process can be initiated and localized around the pre-embedded Pd NPs, resulting in multiple NPs being confined to a single crystal MOF (Metal Organic Framework) particle alone, that is, forming a multi-yolk–shell structure (Fig. 4). The unique structure can effectively prevent the

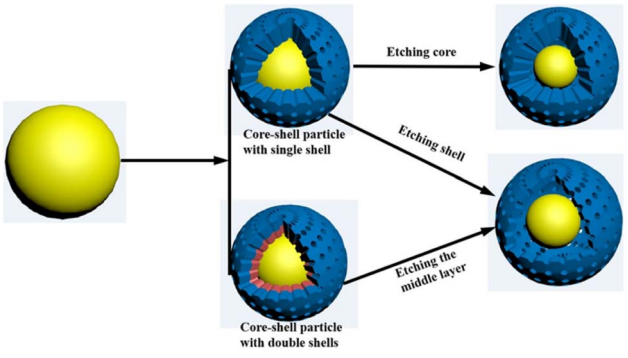

Fig. 2 Illustration of hard template methods for preparing YSNs.

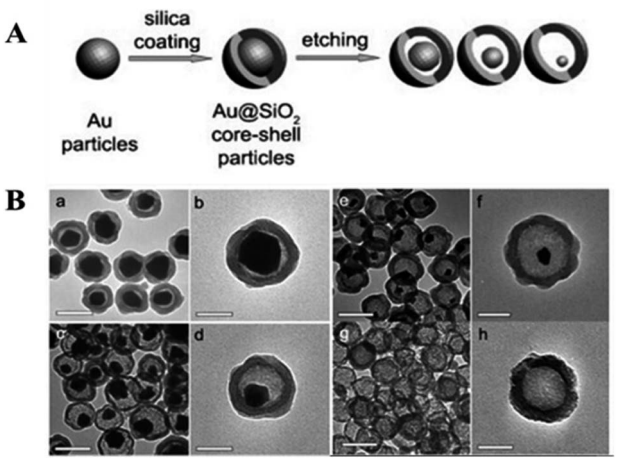

Fig. 3 (A) Synthetic process of Au@SiO_2 nanoreactor framework and (B) TEM images: (a–f) of Au@SiO_2 YNSs, (g, h) silica hollow shells.

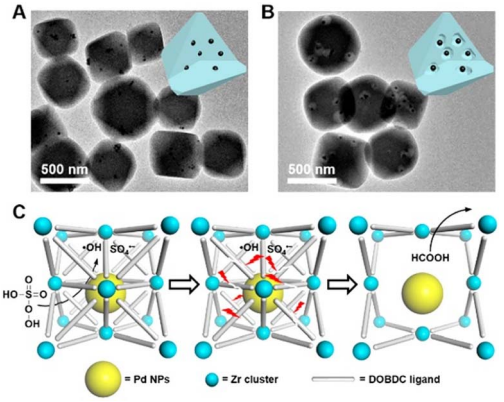

Fig. 4 TEM images of (A) Pd@UiO-66-$(OH)_2$ and (B) MYS-Pd@UiO-66-$(OH)_2$. (C) Schematic illustration of OLC process.

agglomeration of nanoparticles and realize size selective catalysis.[9]

2.1.3 Remove the middle shell. YSNs can also be prepared *via* etching the middle layer from the sandwich structure. Zhu *et al.* used carbon spheres as the templates to prepare rattle-type Fe_3O_4@SiO_2 YSNs.[10] The carbon spheres that adsorbed with iron source were coated with mesoporous silica *via* the StÖber method, after the removal of carbon templates and *n*-octadecyltrimethoxysilane (C18TMS) through calcination and the followed reduction under hydrogen atmosphere, the rattle-type Fe_3O_4@SiO_2 YSNs are obtained. Similarly, Yang *et al.* prepared Si@mesoporous carbon (mC) YSNs with large void exhibiting long cycling stability and superior rate-capability.[11] The commercial silicon nanoparticles were first coated with sacrificial silica layer *via* the StÖber method, followed by coating with a mesoporous silica ($mSiO_2$) shell by the means of surfactant-templating sol–gel approach. Then, Si@mC YSNs were obtained after the pyrolysis and hydrofluoric acid etching of the sacrificial silica layer (Fig. 5). Following this method,

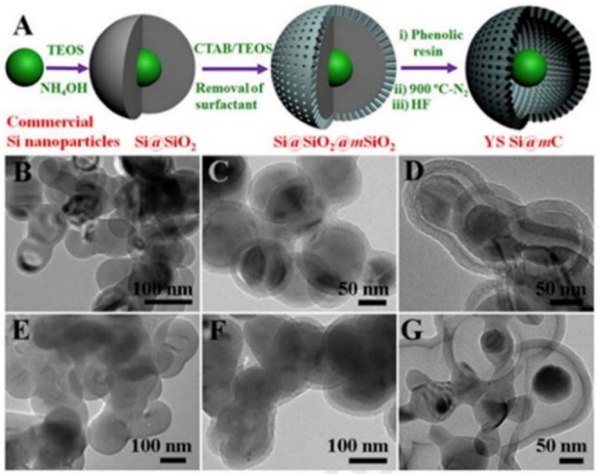

Fig. 5 (A) Schematic illustration of the Si@mC YSNs. (B–G) TEM images of the silica-coated commercial silicon.

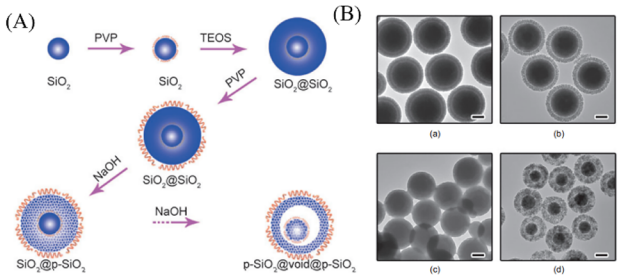

Fig. 6 (A) Illustration of the synthesis of *p*-SiO_2@void@p-SiO_2 YSNs by the surface-protected etching process. (B) TEM images (a–d) of a sample of SiO_2@void@SiO_2 colloids collected at different etching time.

Au@ZrO_2,[12] Fe@porous carbon,[13] and silica nano-rattle YSNs[14] have been successfully synthesized.

2.1.4 Surface-protected etching. In 2008, the method of "surface-protected etching" was put forward by Zhang and co-workers, which includes two major principles:[15] (i) the core particles are coated with a layer of polymeric ligands; (ii) use a suitable etching agent to etch material from the interior of the particles. The polymer chain containing binding groups surround the surface of particles and raise their stability against etching,[16] while selective etching inside the nanoparticles results in the yolk–shell structure. Zhang *et al.* successfully created rattle-type SiO_2@void@SiO_2 structure through this method. Both core and shell are coated with polyvinylpyrrolidone (PVP), followed by NaOH etching. Under the protection of PVP, the core maintains its original property, and the obtained rattle-type colloids have mesoscale pores with two distinct average sizes (Fig. 6).[17]

2.2 Soft template method

Compared with hard template method, the soft template method is a simple, facile and efficient approach for the preparation of inorganic multi-functional YSNs,[18] which overcomes the difficulties related with selective etching, such as multiple steps and accurate control of etchants. When noble metal cores are dispersed in soft template mixture, the soft templates attach to the cores to give well-defined assemblies under certain conditions, which can be regarded as absorbed surfactant layers or microemulsion for the preparation of YSNs, and soft template can be easily removed through washing or calcination.

2.2.1 Surfactant mixtures as the template. Liu *et al.* obtained the hierarchical yolk–shell structure for the first time by encapsulating mesoporous silica NPs into the silica shell by using surfactant mixture as template.[19] As shown in Fig. 7A and B, the core–vesicle complex was prepared by using a fluorocarbon surfactant FC4 and core materials in a mixture of water, ethanol and aqueous ammonia system. Then TEOS is added to deposit silica shell on the surface of the core–vesicle complex, after which the YSNs are formed. Following this method, SiO_2@SiO_2, Au@SiO_2, and Fe_2O_3@SiO_2 YSNs have been obtained by Wu *et al.*[20] For example, the NPs such as SiO_2 and Au are dispersed into a mixture of lauryl sulfonate betaine (LSB)

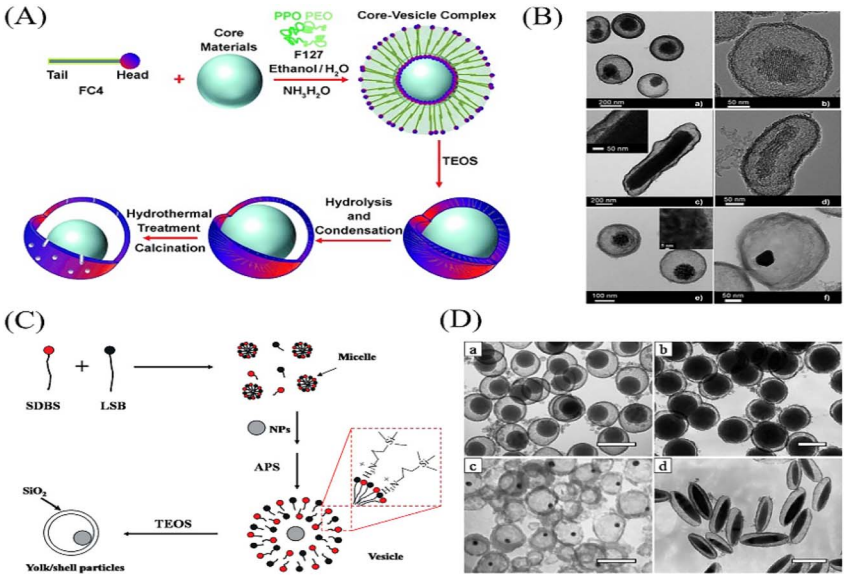

Fig. 7 (A) Procedure for the preparation of yolk–shell structures. (B) TEM images of various yolk–shell materials. (C) Schematic procedure of NP/SiO_2 YSNs. (D) TEM images of yolk/shell structures encapsulated different kinds of NP cores: (a) 90 nm SiO_2 NPs, (b) 220 nm SiO_2 NPs, (c) 10 nm Au NPs, and (d) spindle-like Fe_2O_3 particles.

and sodium dodecyl benzenesulfonate (SDBS), and 3-aminopropyltriethoxysilane (APS) to form the core–vesicle complex followed by the coating of SiO_2 shell (Fig. 7C and D).[20] Thus, we can speculate that by extending this method various NPs@SiO_2 NPs could be produced.

2.2.2 Microemulsion as the template. Microemulsion is a thermodynamically stable monodisperse system which is composed of transparent droplets in oil (W/O) or oil droplets in water (O/W). It is an ordered combination formed by surfactant molecules at the oil/water interface. Microemulsions are usually made up of surfactants, cosurfactant, solvents and water (or aqueous solution).[21] Liu *et al.* synthesized Ag@PSt (polystyrene) YSNs by using the microemulsions as the template, it has two major principles:[22] (1) Ag^+ change into Ag by γ-irradiation *via* inversed microemulsion to form silver nanoparticles; (2) the interfacial-initiated polymerization of styrene. The water-soluble initiator Fe^{2+}–EDTA (ethylenediaminetetraacetate)–SFS (sodium formaldehyde sulfoxylate) react with the oil-soluble initiator CHPO (cumyl hydroperoxide) in the oil–water interface to initiate the polymerization and result in the PSt shell. Zhang *et al.* also demonstrated the preparation of Fe_3O_4@silica YSNs *via* this approach. TritonX-100 is used as surfactant to form a monolayer in W/O microemulsion system, then the first silica shell and outer silica shell are formed by the hydrolysis and condensation of TEOS and *N*-[(trimethoxysilyl)-propyl]poly (PS076) respectively,[23] and finally Fe_3O_4@silica YSNs are obtained after washing and separation (Fig. 8).

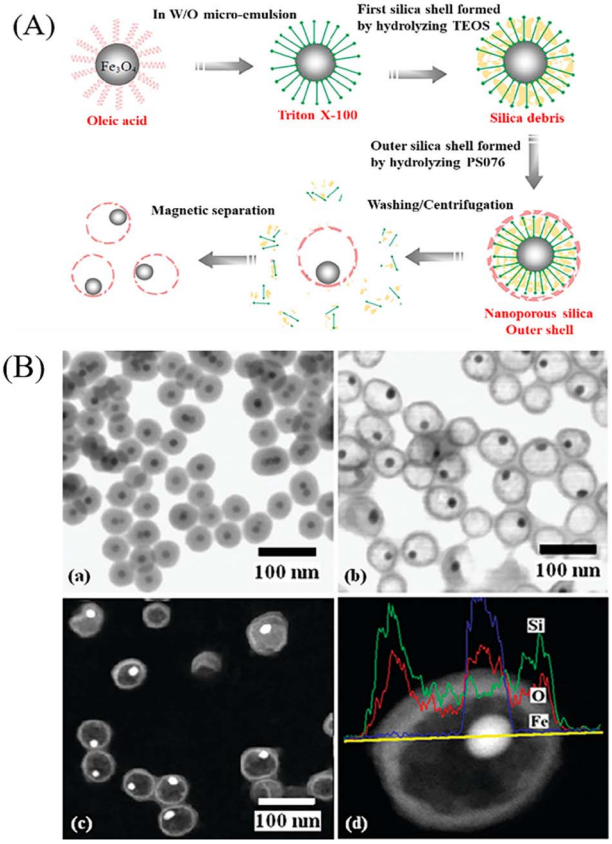

Fig. 8 (A) Schematic diagram for the formation process of Fe_3O_4@-silica YSNs. (B) TEM images of (a) Fe_3O_4@silica and (b) Fe_3O_4@silica YSNs. (c) HAADF-TEM image of Fe_3O_4@silica NPs. (d) EDS analysis along the diameter of the nanoparticle.

2.3 "Ship-in-a-bottle" method

In contrast to the hard template method which can be roughly defined as "from inside to outside", the "ship-in-a-bottle" method is totally opposite which is actually "from outside to inside".[24] The "ship-in-a-bottle" method includes normally

three steps: firstly, the hollow shell as nanoreactor is pre-synthesized. Secondly, loading the core precursors into the hollow shell. Thirdly, the core particles are formed in the hollow cavity through chemical reaction or self-assembly process. In this method, the hollow nanoparticles which act as the nanoreactors will provide a space confinement effect and restrict the growth of core particles inside hollow cavities. According to the formation mechanism, the "ship-in-a-bottle" method can be divided into confined enrichment method and seed-mediated growth method.

2.3.1 Confined enrichment method. The confined self-assembly of guest molecules in hollow structures can be realized by the selective absorption and enrichment of precursor in hollow cavities. For example, the confined growth of MOF nanocrystals in silica shell has been reported by Huang *et al.* Through accurately regulating the structural composition of the hollow material and the microenvironment, the Cu^{2+} can be enriched inside the cavities of the hollow silica sphere, and then the addition of organic ligands to the solution induces the nucleation and growth of MOF in the cavity[25] due to the local higher concentration of metal ions (Fig. 9). Similarly, Qi *et al.* have successfully prepared ZIF-67@HCSs YSNs *via* this method. Hollow carbon nanospheres (HCSs) are pre-synthesized, then a melting-diffusion strategy[26] is used to infiltrate 2-methylimidazole (MI) into the hollow cavities of HCSs (MI@HCSs), followed by the addition of $Co(NO_3)_2$ solution to induce the formation of ZIF-67 inside the hollow carbon nanospheres (Fig. 10A). Qiao *et al.* also used this approach to encapsulate metal clusters in silica shell. Polymer dot@silica core–shell nanoreactors are first formed by the polymerization of ethylenediamine and carbon tetrachloride inside the hollow silica,[27]

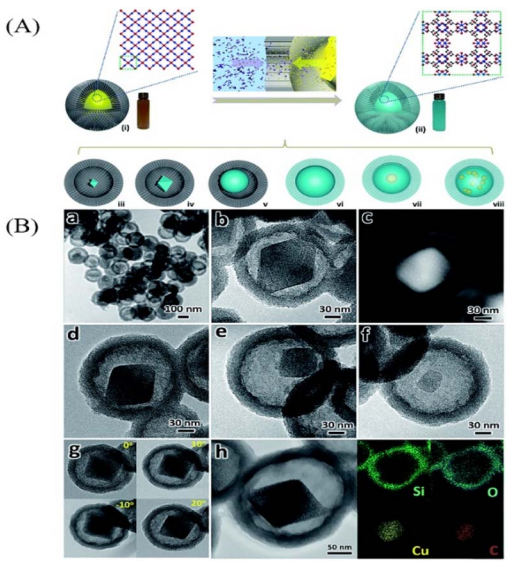

Fig. 9 (A) Synthesis routes for the confined growth of MOF crystals in the $mSiO_2$ shell. (B) Characterization of yolk–shell structured MOF@$mSiO_2$: (a–f) TEM images of the samples prepared at different H_3BTC concentrations; (g) TEM images of the yolk–shell structured MOF@$mSiO_2$ at different tilting angles; (h) EDX elemental maps of the yolk–shell structured MOF@$mSiO_2$.

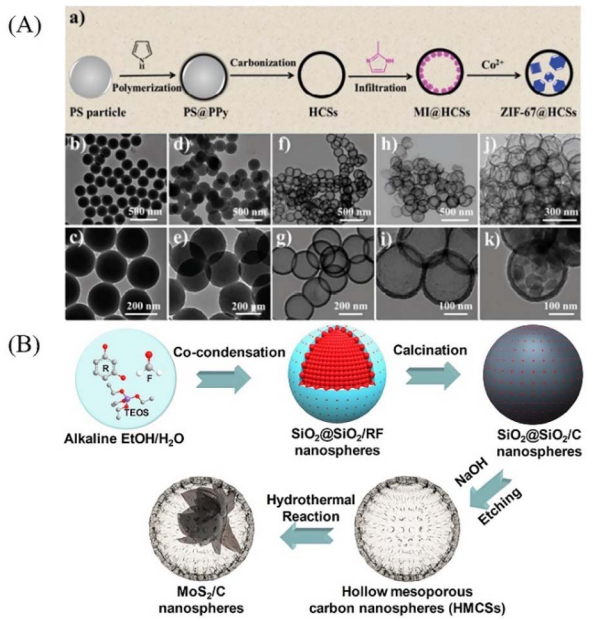

Fig. 10 (A) (a) Synthetic route for the synthesis of ZIF-67@HCSs. TEM images of the products corresponding to each step: (b, c) polystyrene (PS) nanospheres; (d, e) PS@polypyrrole nanospheres; (f, g) HCSs; (h, i) MI@HCSs; and (j, k) ZIF-67@HCSs. (B) Mechanism for the development of MoS_2@C YSNs through confined enrichment method.

then target metal ions can be absorbed at the surface of polymer dots due to the amine groups. After the calcination in the H_2 and air respectively, metal cluster@silica YSNs are obtained.

Following this method, Xiue and co-workers prepared hollow mesoporous carbon spheres (HMCSs) serve as nanoreactors to confine the growth of MoS_2 nanosheets (Fig. 10B).[28] Dai and co-workers also prepared HPW@Hollow S-1 YSNs successfully by this method,[29] Na_2WO_4 and Na_2HPO_4 are smaller than the pore size of silicalite-1 (S-1), so they can penetrate into the cavities of the hollow nanosphere and assemble to form phosphotungstic acid (HPW) nanoparticles which will be confined within the Hollow S-1. Recently, $MoSe_2$@HCNS,[30] ZIF-67@CNCs[31] and M_xP_y@CNCs[32] were also successfully prepared by the confined enrichment method.

2.3.2 Seed-mediated growth method. The seed-mediated growth method is based on the encapsulation of seed inside the hollow cavity, then changing the reaction conditions or adding reducing agents promote the seed growth and nucleation, resulting in the formation of YSNs. It is promised as one of the most effective and flexible method for growing noble metal particles inside hollow microspheres. For example, Pinkhassik and co-workers have synthesized Ag particles@polymer YSNs by using liposomes as nanoreactors which have the aqueous core and the hydrophobic bilayer interior. Liposomes containing monomers (1 : 1 mixture of *tert*-butylstyrene and divinylbenzene) and a photoinitiator (2,2-dimethoxy-2-phenylacetophenone, DMPA) in the bilayer and silver ions in the aqueous core are prepared by hydrating a mixture of lipids and monomers with the aqueous solution of silver nitrate followed by extrusion,[33] then UV light is used to initiate the

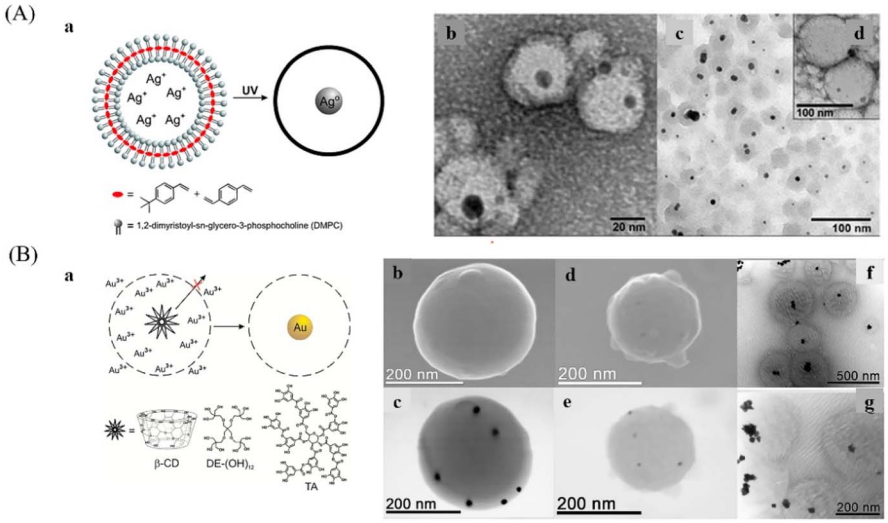

Fig. 11 (A) (a) Synthesis of Ag@polymer YSNs. (b), (c), and (d) TEM images of Ag@polymer YSNs. (B) (a) Initiated synthesis of gold NPs inside hollow porous nanocapsules. SEM image of acrylic (b) and styrene (d) nanocapsules and corresponding STEM images of the same nanocapsules (c, e). (f and g) STEM images of Au NPs synthesized in the presence of KBr inside polystyrene nanocapsules.

polymerization and Ag nanoparticles were formed inside the nanocapsules (Fig. 11A). A similar method was used to prepare Au nanoparticles inside hollow nanocapsules by the reduction of Au^{3+} that pre-trapped in the hollow cavities with reducing agents, such as tannic acid, β-cyclodextrin, and polyether dendrimer,[34] which can be easily fragmented by acid hydrolysis and removed (Fig. 11B).

2.4 Galvanic replacement

Galvanic replacement is a remarkably efficient and facile route to synthesis YSNs with controllable nanostructure, especially for noble metal and metal oxides. The galvanic replacement is mainly focus on the replacement reaction between two metals with different electrical potential, in which the metal with strong activity is used as reducing agent to replace the less active metal from its salt solution. Typically, the core particles coated with anode metal are placed in a cathode salt solution where the dissolving of the anode metal surface and the deposition of the cathode metal on the anode metal surface happens simultaneously, leading to a void between the cathode metal and anode metal.[24] And in fact, the spacing of the voids rely on reaction conditions which could eventually expand towards the center, resulting in a hollow structure. For instance, Sun and coworkers used this method preparing YSNs consisting of Au/Ag alloy core and Au/Ag alloy shell. Two major details can be listed as follows: (1) electroless deposition of a conformal coating of silver on the surface of an Au/Ag alloy nanoparticle; (2) reaction of the resultant particle with an aqueous $HAuCl_4$ solution to replace the coating of silver into Au/Ag alloy shell larger in size.[35] The size of the core, the thickness of the shell and the avoid between the core and shell depend primarily on the amount of $HAuCl_4$ added to the reaction mixture (Fig. 12).

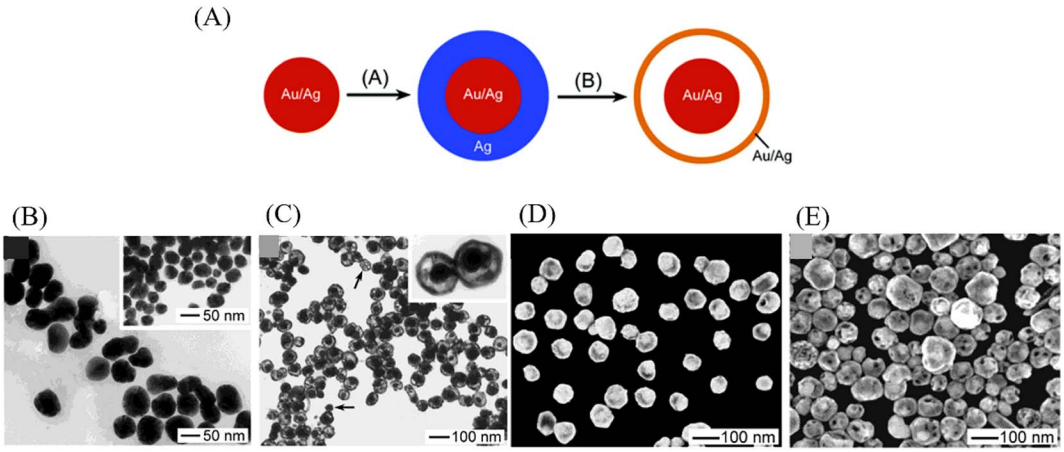

Fig. 12 (A) Schematic illustration of the process for preparing Au/Ag@Au/Ag alloy YSNs. (B) TEM image of Au/Ag alloy colloids. (C) TEM and (D) SEM images of nanorattles. (E) SEM image of another sample that was prepared by increasing the volume of $HAuCl_4$ solution to 0.6 ml.

Similarly, *via* this approach, a Pd@Cu core shell nanocube can be changed into Pb@Au_xCu_{1-x} yolk–shell nanocage, with the further addition of $HAuCl_4$, the Cu shell can be dissolved from the corners toward the interior, after which the cavity will be increasingly enlarged.[36]

2.5 Kirkendall diffusion method

The Kirkendall diffusion is another classical method for YSNs synthesis, which is based on the ion-exchange. However, instead of making use of the different electrical potential, the Kirkendall diffusion occurs at the boundary of two different metals when an imbalance in their diffusion rates appears, leaving vacancies at the material side with the faster diffusion rate. Similar to the galvanic replacement, this approach is also appropriate for the preparation of composites with metal and alloy. As illustrated in Fig. 13A, owing to faster diffusion rate of metal A into B than that of B into A, the alloy (AB) grows in the direction of the faster-moving species (A), which lead to unfilled voids and gaps left in the zone of the faster diffusing component and coalesce into large pores,[37] thus resulting in the YSNs. For example, Cui and co-workers have prepared a kind of yolk–shell Bi@C nanostructures *via* this approach, and the prepared Bi@C YSNs have been proved to be an excellent solid catalyst on the thermal decomposition of cyclotrimethylenetrinitramine.[38] Railsback *et al.* demonstrated the transformation of Ni nanoparticles with different size to hollow or porous NiO through the method of Kirkendall diffusion, Ni diffuse across the Ni/NiO interface and vacancies are formed at the interface and diffuse to the void. The void nucleates when vacancies supersaturate, and the core becomes a small nanoball toward the end of reaction (Fig. 13B).[39]

2.6 Ostwald ripening

Ostwald ripening is a physical phenomenon that refers to the smaller crystal particles produced in the solution will gradually dissolve into the surrounding medium due to their large curvature and high interface energy,[40] and then redeposit onto larger crystalline or sol particles, which further increase the size

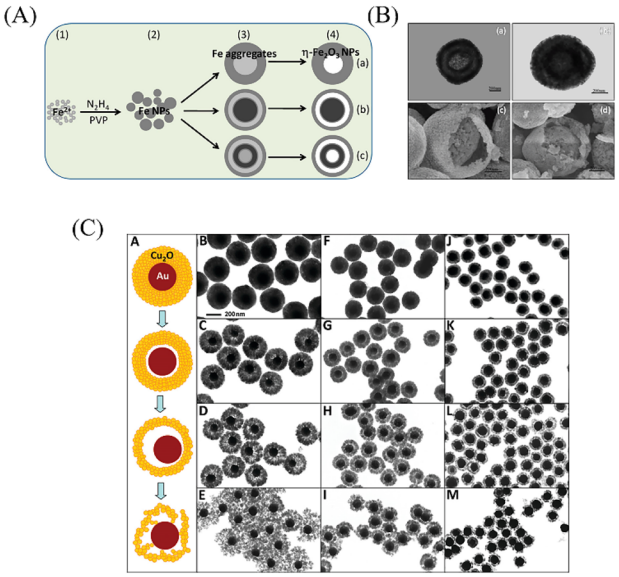

Fig. 14 (A) Schematic for the formation of η-Fe_2O_3 nanoparticles with different interior structures fabricated by the Ostwald ripening process. (B) TEM image of spherical η-Fe_2O_3 nanoparticles (a) and egg-like η-Fe_2O_3 nanoparticles (b) with double-shelled hollow structures. SEM images of two cracked yolk–shell structured η-Fe_2O_3 nanoparticles (c, d). (C) Schematic illustration of the evolution of Au@Cu_2O YSNs.

of the larger crystal particles. This process has recently been widely used in the preparation of YSNs. For example, Zhong *et al.* prepared hollow and yolk–shell structure η-Fe_2O_3 nanoparticles through the Ostwald ripening process. First, hydrazine hydrate is added into the mixture of Fe_3O_4 and poly(vinylpyrrolidone) (PVP) solution, then followed by heating, washing and calcinating,[41] after which the products are collected. By controlling the amount of PVP and reaction time, η-Fe_2O_3 YSNs with spherical, egg-like, olivary elliptical and shuttle-like structures[41] can be easily obtained (Fig. 14A and B). Li *et al.* obtained Au@Cu_2O rattle-like YSNs,[42] *via* the

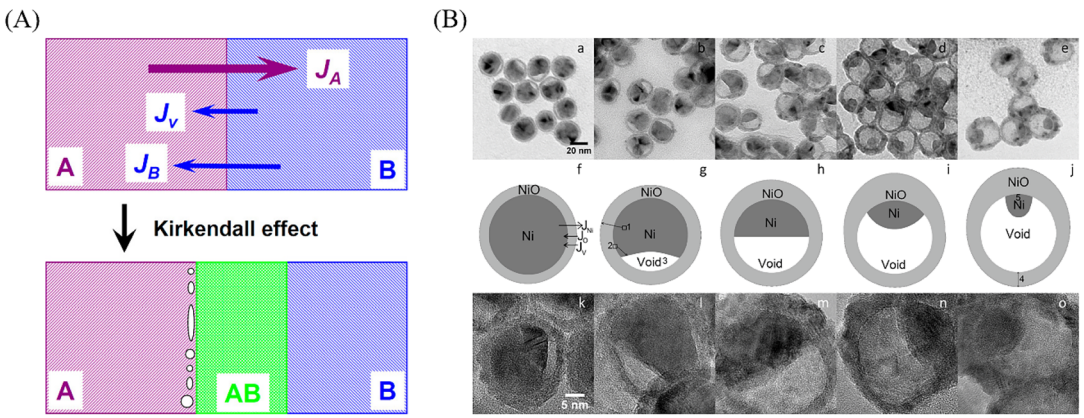

Fig. 13 (A) Schematic diagram of Kirkendall effect (J_A, J_B, and J_v are diffuse fluxes of metal A, B, and void, respectively). (B) TEM images of nanoparticles after oxidation in air at 300 °C for (a) 90, (b) 120, (c) 150, (d) 180, and (e) 210 min. Corresponding oxidation schemes (f–j) and high-resolution TEM images are shown below (k–o).

controllable growth of polycrystalline Cu_2O shell surrounding Au core and the followed the Ostwald ripening of Cu_2O shell (Fig. 14C).

3. Catalytic applications of YSNs

3.1 Chemical catalysis

Due to the unique properties of YSNs, such as low density, movable core, void space between the core and shell, and their readily tailorability and functionality in both the cores and shells, YSNs materials have been widely used as catalysts in many reactions.[43–55] In most of the cases, the movable core of YSNs often serve as catalyst, while the outer shell can not only control the diffusion of the reactants and products, but also provide a confinement effect which prevent particles agglomeration and improve the catalytic performance.

Lv *et al.* reported the use of MOF derived Ni@carbon YSNs as reusable catalysts for reduction of Cr(VI). The results show that Ni@carbon450 exhibit excellent catalytic performance in the presence of HCOOH, and can completely reduce highly toxic Cr(VI) to non-toxic Cr within 30 min, and due to protection effect of the carbon shell, Ni@carbon450 displayed good stability and high catalytic activity after 10 cycles. As described in Fig. 15A, HCOOH and Cr(VI) were firstly adsorbed on the surface of Ni@carbon450 by electrostatic attraction and then Cr(VI) entered the interior of YSNs to reach the active sites. The dehydrogenation decomposition of HCOOH produced H_2 which will be enriched on the surface of the catalyst, and Ni will promote the production of H•, which can readily induce the reduction of Cr(VI) to Cr(III).[56] Fig. 15B shows that pH value and temperature has also a great influence on the catalytic performance. Yu *et al.* used Fe_3O_4@RF (resorcinol formaldehyde) @Au-void@Ys-mPMO (yolk–shell magnetic periodic mesoporous organosilica) to synthesize Au@YS-mPMO with amphiphilic shell, high surface area (393 $m^2\ g^{-1}$), tunable intermediate hollow space (150–156 nm) and high superparamagnetism (34.4–37.1 cmu g^{-1}),[57] which can be used not only as a solid emulsifier to disperse styrene in water, but also as an interface catalyst to convert styrene into styrene oxide with excellent conversion and selectivity of 97.5% and 83.3% respectively (Fig. 16). Dai and co-workers successfully synthesized CeO_2@Pt-Beta YSNs as novel catalysts to improve the H_2 production by LT-ESR (Low Temperature-Ethanol Steam Reforming) reaction. Compared with Pt-Beta and CeO_2–Pt-Beta catalysts, CeO_2@Pt-Beta catalysts show better catalytic performance and excellent stability, the conversion of ethanol is 100% and the selectivity of hydrogen can reach 67%.[58] It is proposed that the ethanol will first enter the interior of the YSNs, then interact with Pt to dehydrogenate to acetaldehyde which will readily decompose into CH_4 and CO. At the same time, SAR ($CH_3CHO + 3H_2O \rightarrow 2CO_2 + 5H_2$) reactions promote the production of H_2, and CeO_2 cores also promotes the WGS ($CO + H_2O \rightarrow CO_2 + H_2$) and ETD ($C_2H_5OH \rightarrow CH_3CHO + H_2$) reaction, resulting in more H_2. Finally, H_2 and CO_2 are purified from the mixed gas by the selectivity of Pt shell.

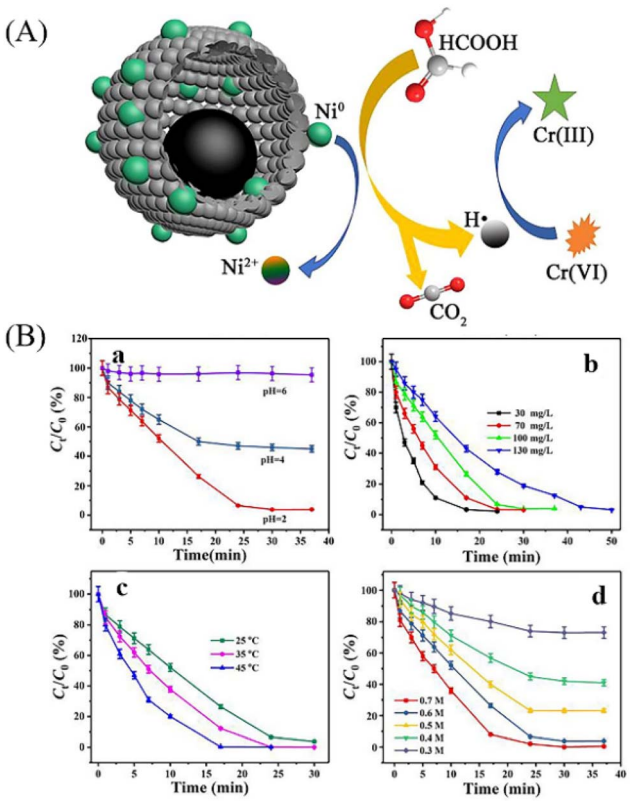

Fig. 15 (A) Cr(VI) reduction mechanism in Ni@carbon450 in the presence of HCOOH system. (B) The effect of pH (a), Cr(VI) concentration (b), temperature (c) and HCOOH concentration (d) on Cr(VI) reduction catalyzed by Ni@carbon450.

Lv *et al.* reported the superior selectivity (47.4%) of Pd@Al_3–$MSiO_2$ YSNs in the hydrogenolysis of glucose to 1,2-propylene glycol (1,2-PG) (Fig. 17A and B). After even 7 times of recycling, the selectivity of 1,2-PG still could reach 38.5% and the conversion of glucose was 90.4% (Fig. 17C).[59] It is proposed that Al atoms can enter mesoporous SiO_2 to form 4-coordinated Al species, which will provide more Lewis acid sites. On the one hand, glucose will be isomerized into fructose in the pores of the shell, and then fructose undergoes retro-aldol condensation in the hollow cavity of the YSNs to generate C3 precursor of 1,2-PG (Fig. 17D). Liu *et al.* prepared YSNs with Ag nanoparticles wrapped in porous Tanus polymer shells composed of hypercrosslinked polystyrene (xPS) and acrylic acid (PAA) brush lining. The porous outer layer of xPS will be beneficial for the diffusion of cationic dyes, and PAA with carboxyl groups show great affinity for cationic dyes, making them easier to be enriched in the cavity of YSNs.[60] The catalytic experiment shows that, under the same experimental conditions, the catalytic performance of Ag@PAA-xPS is much better than that of Ag@xPS, indicating the important role of PAA in the catalyst. Li and coworkers prepared (Pd/C)@Tp(2,4,6-trihydroxybenzene-1,3,5-tricarbaldehyde)Pa(phenylenediamine) COFs(covalent organic frameworks) YSNs for catalyzing the Suzuki reaction. The cut off efficiency of the catalyst for aryl benzene was 100%. When the Pd loading was only as 0.05 mol%, the conversion for aryl benzene was as high as 82%.[50] In addition, the catalyst could be easily recovered by filtration and reused without any

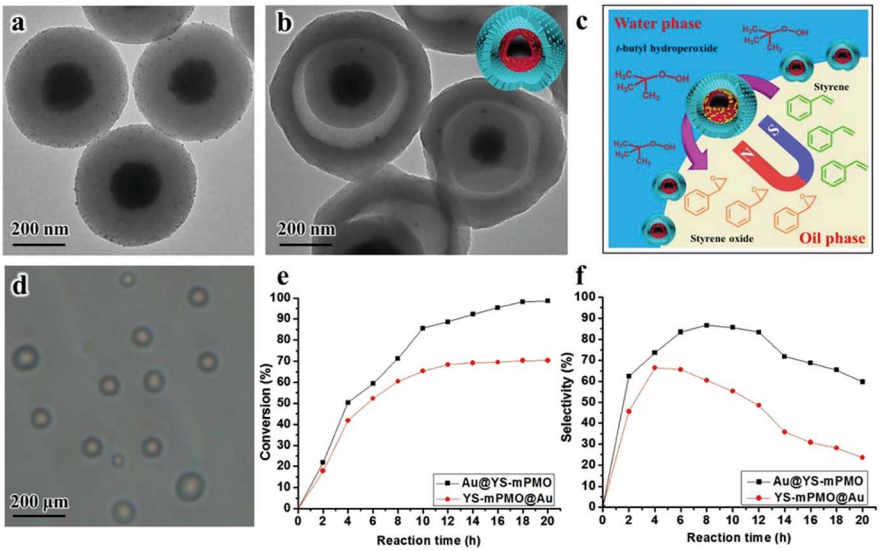

Fig. 16 (a, b) TEM images of Fe_3O_4@RF nanospheres and Au@YS-mPMO YSNs. (c) Microscopic scenario of the reaction occurring on the emulsion platform. (d) The optical microscopy image of the formed pickering emulsion. (e, f) The catalytic performance of the Au@YS-mPMO and YS-mPMO@Au for the epoxidation of styrene at different reaction conditions.

deactivation. The Pd nanoparticles immobilized on the carbon core release Pd atoms to undergo oxidative addition with aryl benzene, and then react with phenylboric acid to produce intermediates (Ar1-Pd-Ar2). Then Pd atoms are captured by the parent Pd core, which catalyzes the completion of the Suzuki reaction. Acharya *et al.* synthesized Au@carbon YSNs which can efficiently catalyze the reduction of 2-amino-4-nitrophenol (NP) to 2,4-diaminophenol (AP).[61] Within 60 min, the deep yellow solution gradually faded, the absorbance at 443 nm (NP) of the UV-Vis absorption spectrum gradually decreased, and a new absorption peak appeared at 320 nm (AP).

3.2 Photocatalysis

Photocatalysis has been regarded as one of the most promising green technologies in chemical conversion, which is driven by the active electrons and holes that generated through

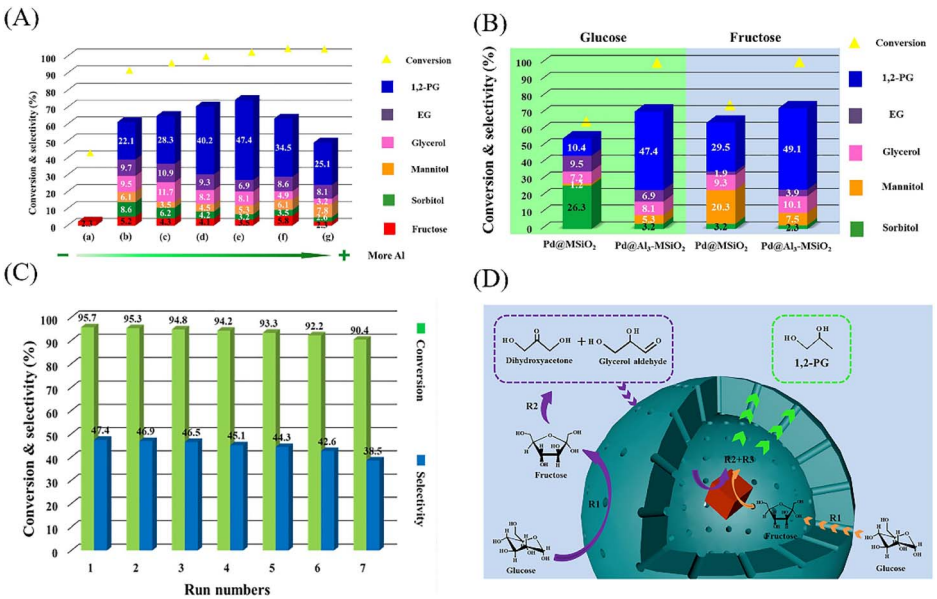

Fig. 17 (A) Activity and selectivity of Pd@Al-$MSiO_2$ YSNSs for glucose hydrogenolysis. (a) blank, (b) Pd@$Al_{0.5}$-$MSiO_2$ YSNSs, (c) Pd@Al_1-$MSiO_2$-YSNSs, (d) Pd@Al_2-$MSiO_2$ YSNSs, (e) Pd@Al_3-$MSiO_2$ YSNSs, (f) Pd@Al_4-$MSiO_2$ YSNSs, (g) Pd@Al_5-$MSiO_2$ YSNSs. (B) The hydrogenolysis of glucose and fructose on Pd@$MSiO_2$ YSNSs and Pd@Al_3-$MSiO_2$ YSNSs. (C) (a) Reusability test in the hydrogenolysis of glucose. (b) TEM image of the Pd@Al_3-$MSiO_2$ YSNSs recovered after the 7th catalytic run. (D) The possible reaction route of glucose hydrogenolysis on Pd@Al-$MSiO_2$ YSNs. R1: isomerization, R2: retro-aldol condensation, R3: hydrogenation.

photoexcitation. Photocatalysts play the most vital role in photocatalysis, thus the research and development of highly efficient photocatalysts is pivotal to the development of photocatalytic technology.[16] Due to the unique architecture and flexible compositions, YSNs can not only enhance light scattering in the hollow space and provide a large specific surface area to create sufficient active sites, but also allow the enrichment of the reactant and provide a homogeneous reaction environment, which minimizes environmental effects in catalytic reactions, achieving improved catalytic performance. In recent years, there are many studies on the preparation of metal oxide@metal oxide yolk–shell structure for photocatalysis. Besides, because Au, Ag, Pd and other noble metal nanoparticles show strong spectral adsorption in the UV-vis band, noble metal@oxide yolk–shell structure show better light absorption and enhance the separation efficiency of electron–hole pairs. In addition, the magnetic materials such as Fe_3O_4 wrapped in semiconductor metal oxide results in magnetic separation performance that can be easily recycled under the action of external magnetic field.[4]

Volatile organic compounds (VOCs) such as formaldehyde, benzene, xylene and lipids often come from the furniture, industrial facilities and construction products and so on.[62] They are not only toxic substances, but also are photochemical reactive with other air pollutants, resulting in secondary pollution, which will cause great harm to environmental quality and human health. Yue *et al.* prepared Au@TiO_2 YSNs for photocatalytic degradation of gaseous toluene under visible light. The degradation rate of gaseous toluene with Au@TiO_2 YSNs was 1.63 times higher than of Au@TiO_2 core–shell nanospheres catalyst and the removal rate of gaseous toluene reached 57% when the concentration of Au@TiO_2 YSNs catalyst was only 0.14 wt% within 3 h,[62] and the catalyst dosage of Au@TiO_2YSNs and C_7H_8 concentration are also explored as factors affecting the degradation efficiency of gaseous toluene (Fig. 18A–D). It is proposed that h^+, $OH^{\bullet}$, $^{\bullet}O^{2-}$, and Ti^{3+} produced in Au@TiO_2 YSNs are the main active components during the reaction. Meanwhile, the separation efficiency of e^-/h^+ pairs was improved by unique yolk–shell structure and localized surface plasmon resonance (LSPR) effect of Au cores, leading to excellent photocatalytic performance (Fig. 18E).

YSNs can also be used as photocatalyst for the degradation of organic pollutants in water, such as dyes,[63–75] pesticides[76] and antibiotics.[77,78] For example, Wang *et al.* reported the preparation of Fe_3O_4@ns-TiO_2/Ag/g-C_3N_4 YSNs which exhibited superior photocatalytic performance for degradation of methyl orange. The reaction rate constant is 0.12723, which is 2.36 times of Fe_3O_4@ns-TiO_2 and 3.64 times of commercial P25.[74] The combination with g-C_3N_4 and the LSPR effect of Ag extend the light response range of TiO_2 to the visible region. Ag located between TiO_2 and g-C_3N_4 can serve as an electron transfer bridge to effectively promote the separation of electron–hole pairs. Xiang and co-workers have prepared $ZnFe_2O_4$@-void@$ZnFe_2O_4$ YSNs with excellent tetracycline (TC) photo-Fenton degradation (Fig. 19A and C). Moreover, they found that the presence of SO_4^{2-} and Cl^- could increase the degradation rate of TC due to the production of radicals ($Cl^{\bullet}$ and $^{\bullet}SO_4^{2-}$) which retarded the combination of electrons and holes (Fig. 19B).[77]

Photocatalytic decomposition of water is one of the most promising and environmentally friendly approach for the production of hydrogen, which is most ideal pollution-free green energy sources in the 21st century. Wang and co-workers fabricated UMT (ultrathin MoS_2 decorated yolk–shell TiO_2) YSNs, in which the ultrathin MoS_2 sheets are evenly embedded on TiO_2. When the loading amount of ultrathin MoS_2 is 0.14 wt%, the photocatalytic hydrogen evolution rate (HER) is 2443 μm g^{-1} h^{-1}, which is 100% and 470% of pristine TiO_2 (247 μ mol g^{-1} h^{-1}) and BMT (bulk MoS_2/TiO_2) (513μ mol g^{-1} h^{-1}).[79] They deposited Pt in UMT-0.14 YSNs (Pt/UMT-0.14), and found that Pt was reduced and grown at the edge of ultrathin MoS_2, which indicates that a large number of photoelectrons exist in ultrathin MoS_2. In addition, they observed that UMT-0.14 still shows stable HER performance after 12 cycles, and long sulfurization time led to a significant decrease in hydrogen production (Fig. 20). The significant enhancement of HER is attributed to the fact that the ultrathin MoS_2 sheets provide sufficient channels to accelerate the transfer of

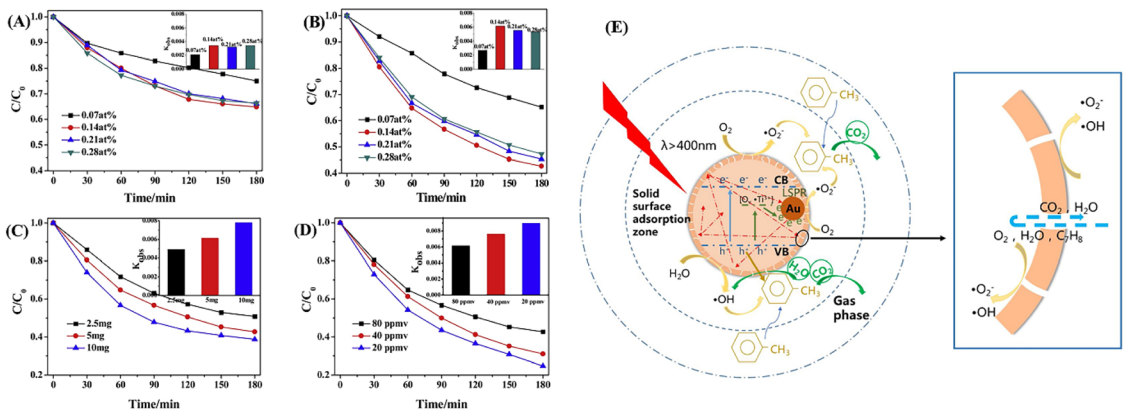

Fig. 18 C_7H_8 photodegradation with different (A) Au content in Au@TiO_2 core–shell nanospheres and (B) Au@TiO_2YSNs, (C) catalyst dosage of Au@TiO_2YSNs and (D) C_7H_8 concentration. (E) The photocatalytic degradation mechanism of Au@TiO_2 YSNs.

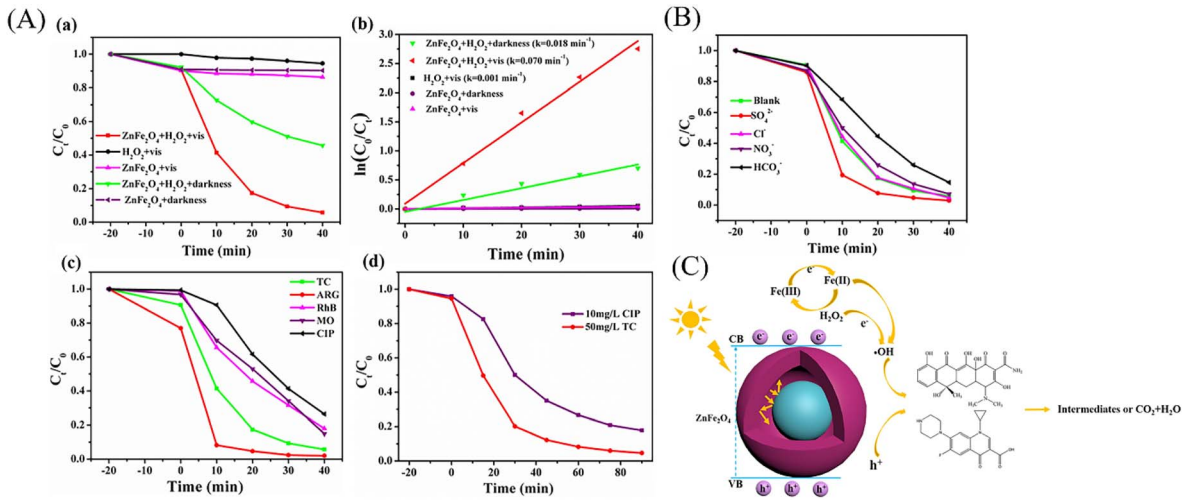

Fig. 19 (A) The (a) TC degradation rates and (b) kinetic curves of prepared samples under different condition, (c) the photo-Fenton degradation activities for different pollutants by $ZnFe_2O_4$@void@$ZnFe_2O_4$ catalyst, (d) the degradation rates for mixed pollutants by $ZnFe_2O_4$@void@$ZnFe_2O_4$ catalyst. (B) Effects of inorganic anions on the photo-Fenton degradation of TC. (C) Photo-Fenton mechanism for TC degradation over the yolk–shell $ZnFe_2O_4$@void@$ZnFe_2O_4$ sphere under visible light irradiation.

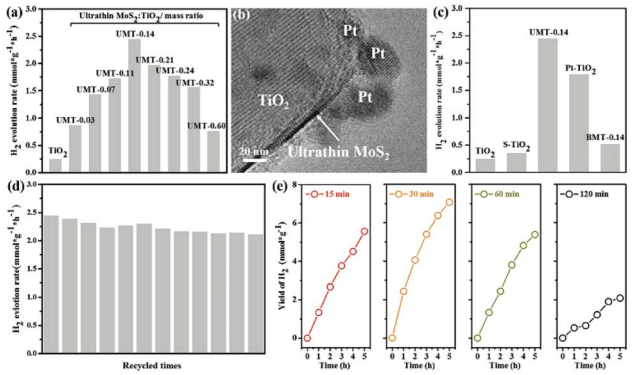

Fig. 20 (a) Photocatalytic H_2 evolution test for MoS_2–TiO_2 composites with different mass ratios of MoS_2; (b) TEM image of Pt/UMT-0.14; (c) photoactivity comparison by various photocatalysts (TiO_2, S–TiO_2, Pt–TiO_2, UMT-0.14, and BMT-0.14); (d) Recycling of photocatalytic HER over UMT-0.14 for twelve consecutive batches; (e) photocatalytic activity of UMT-0.14 samples under different sulfuration time.

photogenerated electrons between the TiO_2 and ultrathin MoS_2, which improve the carrier density (1.97×10^{22} cm^{-3}) and reduces the transfer resistance. Similarly, Zhang *et al.* prepared Cu@Cu_2O YSNS with controllable morphology by changing the concentration of OTAC (octadecyl trimethylammonium chloride).[80] The photocatalytic hydrogen production rate was 97 times higher than that of pure TiO_2, and showed excellent long-term durability.

3.3 Electrocatalysis

With the development of mobile electronics and electric vehicles, lithium-ion batteries with high energy density, high safety, low cost and long-life periods are highly desirable.[81] YSNs with nanoscale void space and functional shells can act as a barrier to prevent the aggregation of the encapsulated electroactive NPs. Moreover, it will offer sufficient space to accommodate the huge volume variation of NPs during the charge/discharge process, which can affect the insertion and detachment of lithium ions and improve the cycling performance. Li *et al.* prepared Fe_3O_4@C–PtRu YSNs as catalysts to enhance the performance of lithium–O_2 battery. When Fe_3O_4@C–PtRu catalyst is used in the cathode of lithium–O_2 battery, the electrochemical performance of the battery has been greatly improved. The battery has a high reversible capacity of 7996 mA h g^{-1} at 200 mA g^{-1}, and the limited capacities of 21 and 32 cycles at 200 mA g^{-1} is 1000 and 500 mA h g^{-1} respectively (Fig. 21A–C).[82] As shown in Fig. 21D, Li_2O_2 discharge products were deposited in the cavity of Fe_3O_4@C–PtRu YSNs after discharge. After recharging, the deposited products disappear, and the Fe_3O_4 core can be observed again, which indicates that the internal void between the shell and core can overcome the volume change in the recharging/discharging process ($2Li + O_2 \leftrightarrow Li_2O_2$) and maintain a good shape of the yolk–shell structure, thereby improving the performance of lithium–O_2 batteries. Wang and co-workers reported that the addition of Fe_2O@N/HCSs into the cathode of Zn–air battery can achieve high open circuit voltage (1.57 V), high power density (140.8 mW cm^{-2}), high specific capacity (726.9 mA h g^{-1}) and excellent long-term cycle performance (300 h) compared with commercial Pt/C + RuO_2 (Fig. 22).[83] Similarly, Kun *et al.* reported the use of $NiCO_2P_x$/rGO YSNs as bidirectional catalysts in the sold–liquid process of advanced lithium–sulfur battery. They claimed that the unique yolk–shell structure exposes more catalytic active sites, which ensure more effective contact between catalysts and polysulfides, and provides sufficient space for sulfur loading and volume variation during the buffer cycle. As a result, the sulfur cathode assembled with $NiCO_2P_x$/rGO has a high capacity of 1238.7 mA h g^{-1} at 0.1 C and still maintains a stable discharge capacity of 561.1 mA h g^{-1} after 400 cycles.[84] Finally, they

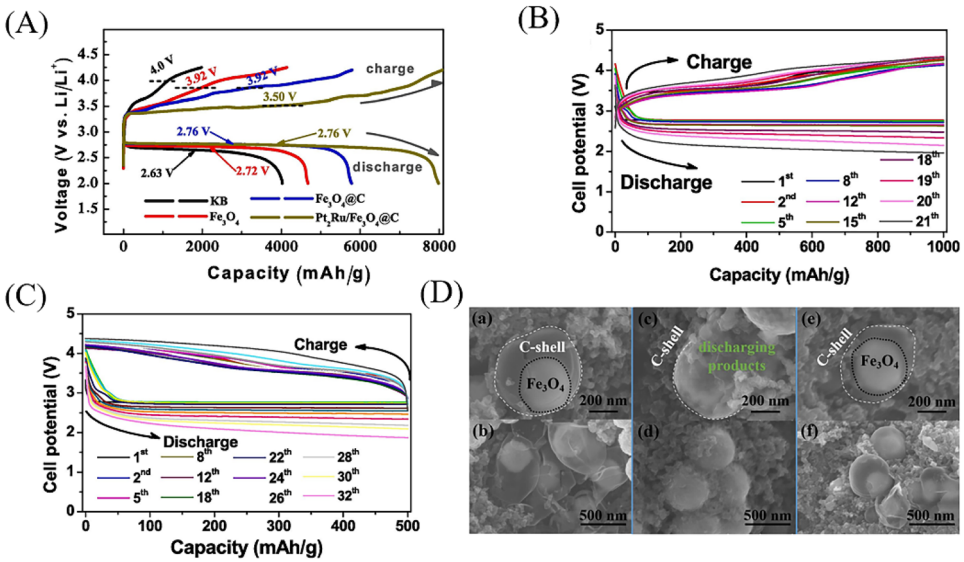

Fig. 21 (A) The initial discharge–charge curves of pure KB, Fe_3O_4, Fe_3O_4@C Fe_3O_4@C–PtRu cathodes at 200 mA g^{-1}. (B) The discharge–charge performance and of the Fe_3O_4@C–PtRu electrodes at 200 mA g^{-1} with curtailing with the capacities to 1000 mA h g^{-1}. (C) The discharge–charge performance of the Fe_3O_4@C–PtRu electrodes at 200 mA g^{-1} with curtailing with the capacities to 500 mA h g^{-1}. (D) The different magnified SEM images of the (a, b) fresh, (c, d) full discharged and (e, f) full re-charged Fe_3O_4@C–PtRu electrodes.

further studied the nucleation and dissolution of Li_2S, the discharging and charging profiles of Li_2S_8 on different surfaces and electrodes confirmed that $NiCO_2P_x$/rGO was an excellent bidirectional catalyst in redox conversion ($Li_2S_x \leftrightarrow Li_2S$).

Electrolytic water is also an environmentally friendly way to produce hydrogen at present. However, the oxygen evolution reaction (OER) involved in electrolytic water is considered to be the main bottleneck to for hydrogen production, since the formation of O–O bond in OER is a $4e^-$ process with slow kinetics and requires high overpotential to reach its reaction barrier.[85–87]

Wang *et al.* designed Fe_2O@N/HCSs YSNs with Fe–N_x active sites as electrocatalysts, which showed excellent ORR (half-wave

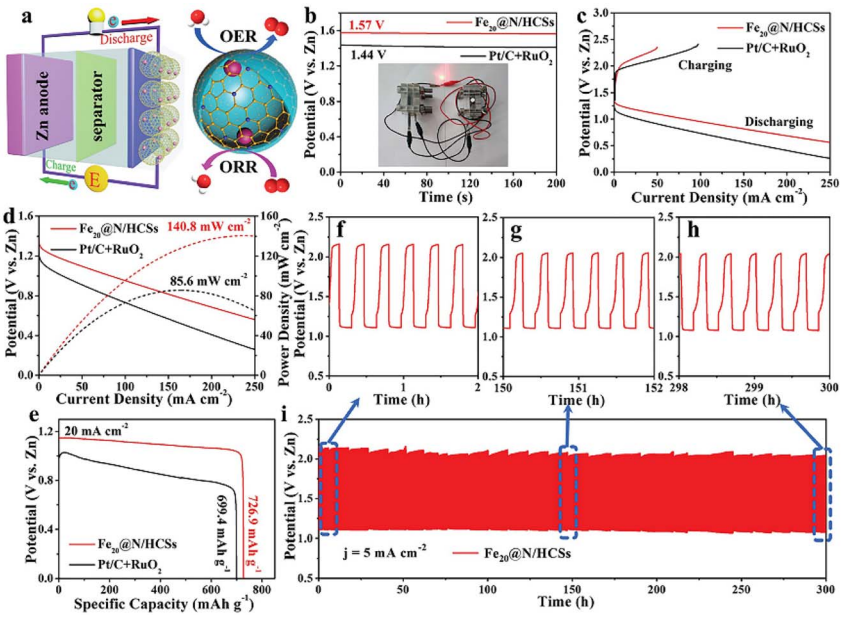

Fig. 22 (a) Schematic illustration of the aqueous Zn–air battery with Fe_2O@N/HCSs as the air cathode. (b) The open-circuit voltage (inset: the optical images of red LED lightened by Zn–air battery based on Fe_2O@N/HCSs), (c) charging–discharging, and (d) power density curves (e) discharge curves at a current density of 20 mA cm^{-2} of Zn–air battery based on Fe_2O@N/HCSs and Pt/C + RuO_2 as air cathode. (f–h) The amplified charge–discharge profiles upon cycling at different testing time. (i) Cycling performance of the rechargeable Zn–air batteries based on Fe_2O@N/HCSs as air cathode.

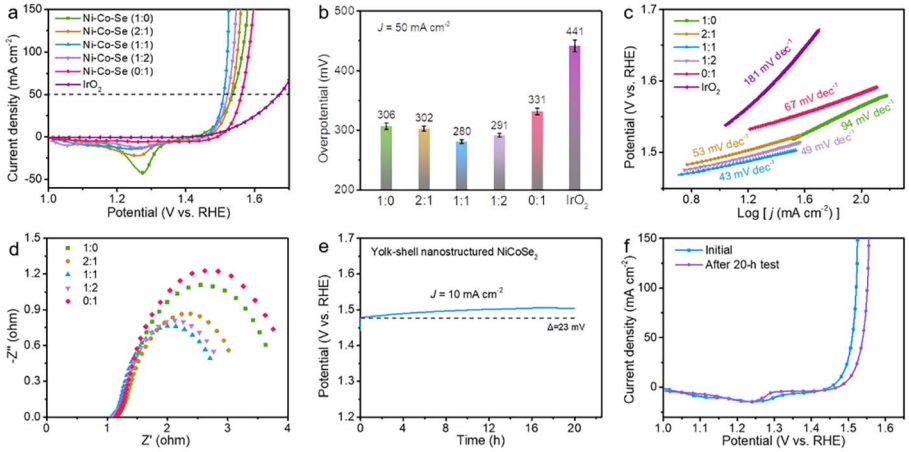

Fig. 23 (a) Polarization curves of the Ni–Co–Se samples with various Ni and Co atomic ratios and the commercial IrO_2. (b) The overpotential contrast for the catalysts at a current density of 50 mA cm^{-2}. (c) The homologous Tafel plot. (d) The corresponding EIS spectra. (e) The chronopotentiometric measurement of $NiCoSe_2$@Se YSNs at a current density of 10 mA cm^{-2}. (f) The polarizations curves of the $NiCoSe_2$ at the initial state and after the electrolysis test.

potential $E^{1/2} = 0.850$ V, Tafel plots = 58.7 mV dec^{-1} and limited current density $J_L = 5.750$ mA cm^{-2}) and OER ($\eta_{10} = 289$ mV, Tafel plots = 52.4 mV dec^{-1}) activity and stability (high relative current of 87.0% after 30 h electrolysis).[83] It is proposed that confinement effect of YSNs with could improve the OER in the hollow cavity and reduced the reaction delay caused by material agglomeration. Besides, Fe_3O_4 nanoparticles embedded in hollow carbon spheres could improve the electrical conductivity of the materials and enhanced the effective distribution of Fe–N_x active sites, thus leading to excellent ORR and OER properties. Similarly, Gan *et al.* synthesized a series of $NiCoSe_2$@Se YSNs based on Kirkendall effect. When the molar ratio of Ni to Co is 1 : 1, $NiCoSe_2$@Se YSNs showed the best OER performance (highest current density at 1.0–1.65 V, low overpotential of 249 mV, lowest contact resistance and charge transfer impedance, small Tafel slope of 43 mV dec^{-1} and tiny decay of 23 mV over 20 h electrolysis) (Fig. 23).[88] They believed that the metal properties of selenide and the high conductivity of Ni enable raid electron transfer between electrode and electrolyte, the wide and hollow annular channel in the unique yolk–shell nanostructure is conducive to the penetration and transportation of electrolyte ions and the exposure of active centers.

4. Conclusions

In this review, we summarize the synthetic methods of YSNs and their applications in the field of chemical catalysis, photocatalysis and electrocatalysis. Despite many different synthetic methods have been developed, there are still many challenges need to be overcome. For instance, for removing the sacrificial layers in hard template method, environment-friendly dissolving or etching agents is urgent desired to avoid using the harmful dissolving solvents such as hydrofluoric acid. In addition, the soft template method cannot well control the uniformity of YSNs. Moreover, it is still lack of a common set of approaches for the fabrication of YSNs, most of which involve multiple steps and work successfully only in specific situations. Exploring more effective, environmentally friendly, universal and low-cost synthetic methods is still our primary research objective. In order to meet the requirements of practical applications, the core and shell of yolk–shell structure need to be selectively functionalized, and YSNs with more complex structure and compositions are required. And a better control of the structure, morphology and function of YSNs deserves further investigation. Finally, more effort should be made to improve the recyclability of YSNs.

When YSNs being used as catalyst, the porosity of the shell can be further adjusted to regulate the diffusion rate of reactants, so as to better control the catalytic performance. Similarly, precise localization of the active sites in YSNs can also improve the catalytic performance. For example, due to the continuous movement of yolk core particles in a photocatalytic process, where complex charge transfer and separation are required, a rational design of the charge transfer mechanism between yolk and shell will be a key future research direction. Meanwhile, in the core and shell region, the spatial separation of photogenerated electrons and holes is very difficult which requires a new breakthrough. In addition, yolk–shell nanostructures are expected to be used as electrocatalysts to improve battery performance in the near future, especially when commercial processes are established. Nevertheless, the application of YSNs in more research fields needs to be explored.

Conflicts of interest

The authors declare no conflict of interest.

Acknowledgements

This work is supported by the Natural Science Foundation of Shandong Province of China (No. ZR2022MB136) and the Scientific Research Fund of Heze University (No. XY20BS18).

References

1 C. A. H. Price, T. R. Reina and J. Liu, *J. Energy Chem.*, 2021, **57**, 304–324.
2 X. Sun, J. Han and R. Guo, *Front. Chem.*, 2020, **8**, 1135–1143.
3 G. M. Ziarani, P. Mofatehnia, F. Mohajer, *et al.*, *RSC Adv.*, 2020, **10**, 30094–30109.
4 D. Du, W. Shi and L. Wang, *Appl. Catal. B Environ.*, 2017, **200**, 484–492.
5 M. Wang, Y. Boyjoo and J. Pan, *Chin. J. Catal.*, 2017, **38**, 970–990.
6 J. He, L. Luo and Y. Chen, *Adv. Mater.*, 2017, **29**, 1702707–1702711.
7 J. Lee, J. C. Park and H. Song, *Adv. Mater.*, 2008, **20**, 1523–1528.
8 W. S. Choi, H. Y. Koo and D. Y. Kim, *Langmuir*, 2008, **24**, 4633–4636.
9 L. Luo, W. S. Lo, X. Si, *et al.*, *J. Am. Chem. Soc.*, 2019, **141**, 20365–20370.
10 Y. Zhu, E. Kockrick and T. Ikoma, *Chem. Mater.*, 2009, **21**, 2547–2553.
11 J. Yang, Y. Wang and S. Chou, *Nano Energy*, 2015, **18**, 133–142.
12 P. M. Arnal, M. Comotti and F. Schüth, *Angew. Chem., Int. Ed.*, 2006, **45**, 8224–8227.
13 W. Qingqing and L. Wei, *Chem.–Eur J.*, 2018, **24**, 15663–15668.
14 C. Dong, L. Li and F. Tang, *Adv. Mater.*, 2009, **21**, 3804–3807.
15 Q. Zhang, T. Zhang and J. Ge, *Nano Lett.*, 2008, **8**, 2867–2871.
16 R. Purbia and S. Paria, *Nanoscale*, 2015, **7**, 19789–19873.
17 Q. Zhang, J. Ge and J. Goebl, *Nano Res.*, 2009, **2**, 583–591.
18 L. S. Lin, J. Song and H. H. Yang, *Adv. Mater.*, 2018, **30**, 1701–4639.
19 J. Liu, S. Z. Qiao and S. Budi Hartono, *Angew. Chem., Int. Ed.*, 2010, **49**, 4981–4985.
20 X. J. Wu and D. Xu, *J. Am. Chem. Soc.*, 2009, **131**, 2774–2775.
21 K. A. Dahlberg and J. W. Schwank, *Chem. Mater.*, 2012, **24**, 2635–2644.
22 W. J. Liu, Z. C. Zhang, W. D. He, *et al.*, *J. Solid State Chem.*, 2006, **179**, 1253–1258.
23 X. Zhang, L. Clime and H. Roberge, *J. Phys. Chem. C*, 2011, **115**, 1436–1443.
24 R. Purbia and S. Paria, *Nanoscale*, 2015, **7**, 19789–19873.
25 Z. Huang, L. L. Fan and B. Chen, *J. Mater. Chem. A*, 2021, **9**, 3976–3984.
26 L. Qi, J. Guo and Z. Hai, *Small*, 2019, **15**, 1804874–1804881.
27 Z. A. Qiao, P. Zhang and S. H. Chai, *J. Am. Chem. Soc.*, 2014, **136**, 112601–112607.
28 Z. Xiue and C. Ming, *ACS Nano*, 2017, **11**, 8429–8436.
29 C. Dai, A. Zhang and J. Li, *Chem. Commun.*, 2014, **50**, 4846–4848.
30 L. Hui, G. Hong and B. Liu, *Adv. Funct. Mater.*, 2018, 1707480–1707488.
31 X. Lu, A. Liu and Y. Zhang, *ACS Appl. Energy Mater.*, 2020, **3**, 11153–11163.
32 W. Li, R. Zhao and K. Zhou, *J. Mater. Chem. A*, 2019, **7**, 8443–8450.
33 S. N. Shmakov and E. Pinkhassik, *Chem. Commun.*, 2010, **46**, 7346–7348.
34 S. N. Shmakov, Y. Jia and E. Pinkhassik, *Chem. Mater.*, 2014, **26**, 1126–1132.
35 Y. Sun, B. Wiley and Z. Y. Li, *J. Am. Chem. Soc.*, 2004, **126**, 9399–9406.
36 S. Xie, M. Jin and J. Tao, *Chem.–Eur. J.*, 2012, **18**, 14974–14980.
37 W. Wang, M. Dahl and Y. Yin, *Chem. Mater.*, 2013, **25**, 1179–1189.
38 C. M. Cui, X. H. Guo, Y. M. Geng, T. T. Dang, G. Xie, S. P. Chen and F. Q. Zhao, *Chem. Commun.*, 2015, **51**, 9276–9279.
39 J. G. Railsback, A. C. Johnston-Peck and J. Wang, *ACS Nano*, 2010, **4**, 1913–1920.
40 Y. A. Chen, Y. T. Wang and H. S. Moon, *RSC Adv.*, 2021, **11**, 12288–12305.
41 J. Zhong, C. Cao and H. Liu, *Ind. Eng. Chem. Res.*, 2013, **52**, 1303–1308.
42 Z. Li, D. A. Blom and W. Hui, *Chem. Mater.*, 2011, **23**, 4587–4598.
43 J. Sun, J. Hu and J. Han, *Langmuir*, 2019, **35**, 1–30.
44 X. Du, C. Zhao and Y. Luan, *J. Mater. Chem. A*, 2017, **5**, 21560–21569.
45 Y. Zhuang, S. Yuan and J. Liu, *Chem. Eng. J.*, 2019, **379**, 122262–122270.
46 Q. C. Do, D. G. Kim and S. O. Ko, *Environ. Res.*, 2019, **171**, 92–100.
47 G. Yuan, J. Sun and X. Sun, *Colloids Surf., A*, 2021, **623**, 126665–126672.
48 A. Acharya, A. Kumar and I. S. Lee, *Bull. Korean Chem. Soc.*, 2021, **42**, 915–918.
49 S. Gao, L. Zhang and H. Yu, *Carbon*, 2021, **175**, 307–311.
50 Y. Li, B. Pei and J. Chen, *J. Colloid Interface Sci.*, 2021, **591**, 273–280.
51 Y. Guo, L. Feng and C. Wu, *ACS Appl. Mater. Interfaces*, 2019, **11**, 33978–33986.
52 R. Cai, H. Jin and D. Yang, *Nano Energy*, 2020, **71**, 104542–104548.
53 F. Shaik, *ChemNanoMat*, 2020, **6**(10), 1449–1473.
54 Y. Lu, D. Guo and Y. Ruan, *J. CO2 Util.*, 2018, **24**, 190–199.
55 S. Prabu and K. Y. Chiang, *J. Colloid Interface Sci.*, 2021, **604**, 584–595.
56 Z. Lv, X. Tan and C. Wang, *Chem. Eng. J.*, 2020, **389**, 123428–123436.
57 L. Yu, P. Pan and Y. Zhang, *Small*, 2019, 1805465–1805473.
58 R. Dai, Z. Zheng and C. Lian, *Int. J. Energy Res.*, 2019, **43**, 2075–2085.
59 M. Lv, Y. Zhang and Q. Xin, *Chem. Eng. J.*, 2020, **396**, 125274–125285.
60 S. Liu, Y. Lin and W. Guo, *Chin. J. Polym. Sci.*, 2020, **38**, 847–852.
61 A. Acharya, A. Kumar and I. S. Lee, *Bull. Korean Chem. Soc.*, 2021, **42**, 915–918.

62 Y. Wang, C. Yang and A. Chen, *Appl. Catal. B Environ.*, 2019, **251**, 57–65.
63 M. Ma, Y. Yang and W. Li, *J. Alloys Compd.*, 2019, **810**, 151807–151816.
64 H. Sun, Q. He and P. She, *J. Colloid Interface Sci.*, 2017, **505**, 884–891.
65 Y. Zhang, Y. Zhao and J. Li, *Inorg. Chem. Front.*, 2018, **5**(12), 3082–3090.
66 Y. Zhang, L. Wang and M. Yang, *Appl. Surf. Sci.*, 2019, **466**, 515–524.
67 J. Zhao, S. Tian and H. Shi, *Adv. Mater. Interfac.*, 2019, **6**, 1801933–1801945.
68 J. Feng, J. Liu and X. Cheng, *Adv. Sci.*, 2018, **5**, 1700376–1700382.
69 J. Lu, L. Lan and X. T. Liu, *Front. Chem. Sci. Eng.*, 2019, **13**, 665–671.
70 Q. Li, F. Wang and L. Sun, *Nano-Micro Lett.*, 2017, (9), 131–139.
71 Z. A. Jian, B. Wl and B. Hl, *Adv. Powder Technol.*, 2019, **30**, 1965–1975.
72 C. Rui, J. Lu and S. Liu, *J. Mater. Sci.*, 2018, **53**, 1–10.
73 Z. Zhao, J. Liu and M. Qin, *J. Nanosci. Nanotechnol.*, 2019, **20**, 3140–3147.
74 Y. Lv, L. Yue and I. M. Khan, *Nano Res.*, 2021, **14**, 2363–2371.
75 M. Farbod and L. Sharif, *Phys. B*, 2021, **613**, 412729–412736.
76 I. Khan, N. Sun and Y. Wang, *Mater. Res. Bull.*, 2020, **127**, 110857–110863.
77 Y. Xiang, Y. Huang and B. Xiao, *Appl. Surf. Sci.*, 2020, **513**, 145820–145831.
78 Y. Xing, S. Tang and X. Du, *Nano Res.*, 2020, **14**, 1–6.
79 W. Wang, S. Zhu and Y. Cao, *Adv. Funct. Mater.*, 2019, **29**, 1901958–1901968.
80 H. Zhang, Y. Ma and Z. Liu, *Colloids Surf., A*, 2021, **629**, 127451–127460.
81 G. D. Moon, *Nanomaterials*, 2020, **10**, 675–698.
82 J. Li, L. Chen and R. Ye, *Appl. Surf. Sci.*, 2020, **507**, 145103–145109.
83 B. Wang, Y. Ye and L. Xu, *Adv. Funct. Mater.*, 2020, **30**, 2005834–2005841.
84 Z. Kun, Z. ZX and R. ZW, *ChemElectroChem*, 2021, **8**, 1605–1611.
85 M. Yang, D. Wu and D. Cheng, *Int. J. Hydrogen Energy*, 2019, **44**, 6525–6534.
86 G. Mei, *Electrochim. Acta*, 2018, **290**, 82–89.
87 A. Annamalai, D. V. Shinde and J. Buha, *J. Mater. Chem. A*, 2021, **9**, 10385–10392.
88 L. Lv, Y. Gan and H. Wan, *Int. J. Hydrogen Energy*, 2021, **46**, 28387–28396.